CERN-ACC-2016-0050

# EuCARD-2

Enhanced European Coordination for Accelerator Research & Development

## Journal Publication

# Localization of ionization-induced trapping in a laser wakefield accelerator using a density down-ramp

Hansson, M. (Lund University) *et al*

23 March 2016


The EuCARD-2 Enhanced European Coordination for Accelerator Research & Development project is co-funded by the partners and the European Commission under Capacities 7th Framework Programme, Grant Agreement 312453.

This work is part of EuCARD-2 Work Package **13: Novel Acceleration Techniques (ANAC2)**.

The electronic version of this EuCARD-2 Publication is available via the EuCARD-2 web site <http://eucard2.web.cern.ch/> or on the CERN Document Server at the following URL: <http://cds.cern.ch/search?p=CERN-ACC-2016-0050>

CERN-ACC-2016-0050

Localization of ionization-induced trapping in a laser wakefield accelerator using a density down-ramp



2016 Plasma Phys. Control. Fusion 58 055009

(http://iopscience.iop.org/0741-3335/58/5/055009)

OPEN ACCESS
IOP Publishing
Plasma Physics and Controlled Fusion
Plasma Phys. Control. Fusion **58** (2016) 055009 (7pp)
doi:10.1088/0741-3335/58/5/055009

# Localization of ionization-induced trapping in a laser wakefield accelerator using a density down-ramp

**M Hansson[1], T L Audet[2], H Ekerfelt[1], B Aurand[1], I Gallardo González[1], F G Desforges[2], X Davoine[3], A Maitrallain[4], S Reymond[1,5], P Monot[4], A Persson[1], S Dobosz Dufrénoy[4], C-G Wahlström[1], B Cros[2] and O Lundh[1]**

[1] Department of Physics, Lund University, PO Box 118, 22100 Lund, Sweden
[2] Laboratoire de Physique des Gaz et des Plasmas, CNRS, Univ. Paris-Sud, Université Paris-Saclay, 91405 Orsay, France
[3] CEA, DAM, DIF, Bruyères-le-Châtel, 91297 Arpajon, France
[4] Laboratoire Interactions, Dynamique et Lasers, CEA, Université Paris-Saclay, 91191 Gif-sur-Yvette, France
[5] ENSTA ParisTech, Université Paris-Saclay, 828 boulevard des Maréchaux, 91762 Palaiseau, France

E-mail: martin.hansson@fysik.lth.se

Received 19 February 2016
Accepted for publication 26 February 2016
Published 23 March 2016

**Abstract**

We report on a study on controlled trapping of electrons, by field ionization of nitrogen ions, in laser wakefield accelerators in variable length gas cells. In addition to ionization-induced trapping in the density plateau inside the cells, which results in wide, but stable, electron energy spectra, a regime of ionization-induced trapping localized in the density down-ramp at the exit of the gas cells, is found. The resulting electron energy spectra are peaked, with 10% shot-to-shot fluctuations in peak energy. Ionization-induced trapping of electrons in the density down-ramp is a way to trap and accelerate a large number of electrons, thus improving the efficiency of the laser-driven wakefield acceleration.

Keywords: laser, wakefield, trapping, down-ramp, ionization

(Some figures may appear in colour only in the online journal)

## 1. Introduction

With the breakthrough in 2004 [1–3], the research on laser wakefield accelerators [4] has shown the possibility of generating beams of relativistic electrons with peaked electron energy spectra. The energy of the electrons in the beams depends strongly on the laser system in use, but also on other experimental parameters, such as length and density of the interaction medium, with energies ranging from a few tens of keV [5] up to a few GeV [6]. Much effort is now focused on controlling the properties of the generated beams [7], such as the energy and number of accelerated electrons as well as the divergence and pointing, and on reducing the shot-to-shot fluctuations of these beams [8]. Several techniques to control the injection and trapping of electrons in an excited plasma wave have been demonstrated experimentally to decrease the shot-to-shot fluctuations in charge and energy of the electrons in the generated beams. These methods include trapping by colliding pulses [9], trapping in density transitions [10, 11] and down-ramps [7, 12, 13] and ionization-induced trapping [14, 15].

Trapping of electrons in a density down-ramp is similar to the mechanism of self trapping, which occurs when the electrons that constitute the plasma wave approach and exceed the phase velocity of the wave. In a density down-ramp the phase velocity of the plasma wave behind the driving laser pulse is decreased and the threshold for trapping is thereby



 

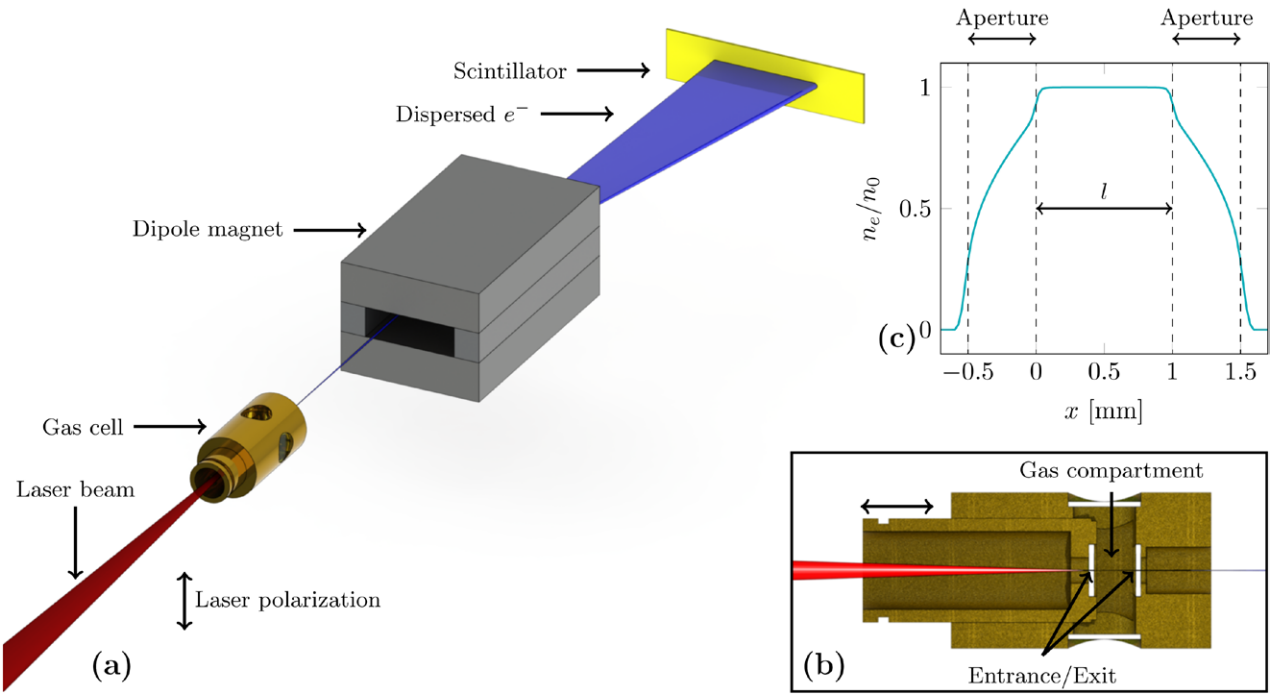


**Figure 1.** Schematic illustration of the experimental set-up. The laser pulses are focused, through an entrance aperture, into a cell filled with gas. The electrons, accelerated in the interaction, propagate along the optical axis and are then dispersed by a dipole magnetic field before impacting on a scintillating screen and recorded with a 16-bit CCD-camera. (b) Detailed cross section view of the gas cell. The gas cell allows the length to be varied under vacuum during the experiment. (c) Density distribution along the optical axis of the laser beam. The dashed lines marks the entrance and exit apertures through the windows confining the gas, and $l$ is the inner length of the cell, i.e. the distance between the inner surfaces of the windows. The density gradients are characterized using computational fluid dynamics.

also decreased. A drawback of using this technique is that the amount of charge in the bunches of accelerated electrons is relatively small as compared to other mechanisms for injection.

The method of ionization-induced trapping is instead based on the release of free electrons, by field ionization of ions, close to the peak of the laser pulse inside the first period of the excited plasma wave. In contrast to trapping due to a density down-ramp, beams containing a large number of electrons are typically observed when using ionization-induced trapping. However, this type of trapping typically occurs over an extended length, and the electron energy distribution is therefore usually wide. Methods to localize ionization-induced injection and thereby generate quasi-monoenergetic electron energy spectra are certainly of interest including self-truncation of ionization-induced trapping and ionization-induced trapping in a shock [16, 17].

In this paper we present an experimental study, supported by particle-in-cell simulations, on controlled trapping of electrons using a combination of the mechanisms described above. This way, the advantage of higher charge due to ionization-induced trapping is combined with the localization of trapping in a density down-ramp, to produce peaked spectra with high charge. The accelerated beams of relativistic electrons are shown to be reproducible with respect to charge and energy.

## 2. Experimental setup

Experiments are conducted using the multi-terawatt laser at the Lund Laser Centre, based on chirped pulse amplification (CPA) in Ti:sapphire crystals. The duration of the laser pulses, when fully re-compressed after amplification, that are used in this experiment is $(37 \pm 3)$ fs full width at half maximum (FWHM) and each pulse contains approximately $(585 \pm 60)$ mJ of energy. The pulses are focused using an off-axis parabolic mirror with an effective focal length of 0.75 m. Furthermore, closed loop wave-front optimization is performed using a wave-front sensor (Phasics SID4) and a deformable mirror in the beam line. With this optimization the focal spot is almost circularly symmetric with a diameter of 17 $\mu$m (FWHM).

From the measured pulse duration and energy together with images of the focused laser pulse, the peak intensity is estimated to $(3.0 \pm 0.5) \times 10^{18}$ W cm$^{-2}$ when the laser pulse is focused in vacuum, corresponding to a peak normalized vector potential $a_0 = 1.2 \pm 0.1$.

The leakage through the final dielectric folding mirror of a co-propagating reference beam is focused using a lens, and the focal plane is imaged onto a camera. The images of the focus of the reference beam is used, together with a piezo-electrically actuated mirror, to lock the position of the focused pulses and thus prevent long term drifts of the pointing.

The laser pulses are focused through an entrance aperture, with a diameter of either 100 $\mu$m or 200 $\mu$m, into a gas cell of variable length (see figures 1(a) and (b)). The gas cell is mounted using a 5-axis holder to allow accurate positioning of the cell along the optical axis, with the entrance of the cell at the beam waist. Gas is filled from a reservoir through an electronically controlled valve that is opened well before the laser pulse arrives at the target, to reach a stationary density of gas

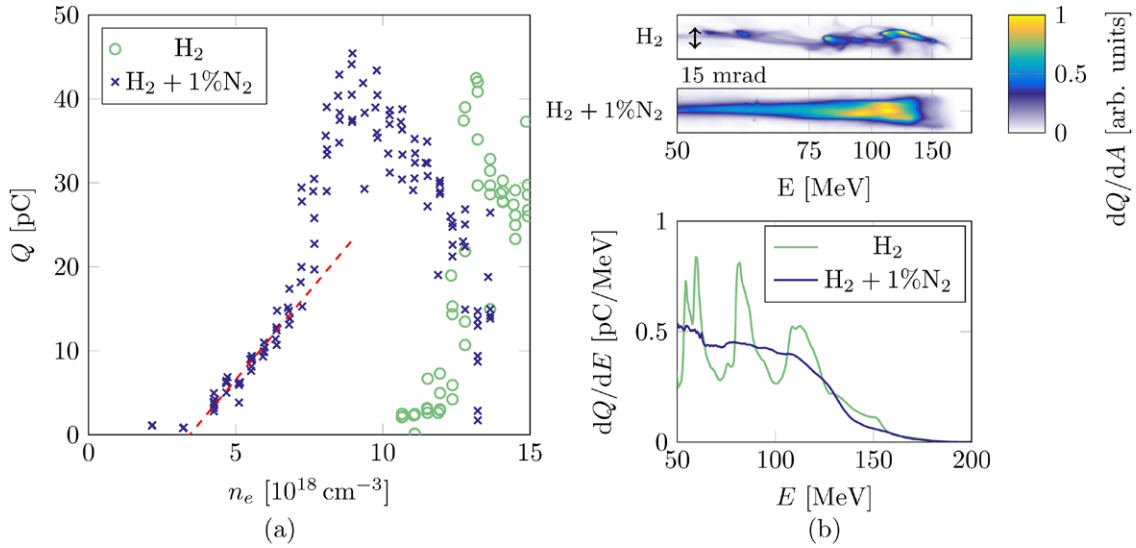


**Figure 2.** (a) Accelerated charge as a function of electron number density in the density plateau of the cell with the inner length set to 2 mm. The threshold in electron number density is clearly lower when 1% of nitrogen is present in the gas as compared to pure hydrogen. Furthermore the threshold for trapping is not as sharp as when pure hydrogen is used. The red dashed line is fitted to the accelerated charge using the gas mixture at electron number densities between $4 \times 10^{18}$ cm$^{-3}$ and $7 \times 10^{18}$ cm$^{-3}$. (b) Typical shape of dispersed electron beams of electrons, and corresponding spectra, accelerated in the gas mixture and in pure hydrogen for beams containing approximately 40 pC of charge. The electron number density is set to $9 \times 10^{18}$ cm$^{-3}$ when the gas mixture is used and $13 \times 10^{18}$ cm$^{-3}$ when pure hydrogen is used. The colormap in each image is normalized to its maximum value. The beams of electrons accelerated in the gas mixture typically have a large divergence and a wide electron energy spectrum whereas the beams of electrons accelerated in pure hydrogen typically consist of multiple peaked features.

in the cell. The number density of neutral gas molecules was characterized using interferometry as a function of backing pressure off-line before the experiment started. Furthermore, the density gradients at the entrance and exit were characterized using computational fluid dynamics simulations (using both OpenFOAM SonicFOAM solver and COMSOL CFD). The length of the gradients (from 10% to 90% of the plateau density) are between 0.5 mm and 0.7 mm depending on the size of the apertures. The normalized gas density distribution along the optical axis of the laser beam is shown in figure 1(c).

To compare self-trapping with ionization-induced trapping, two types of gases are used in the experiment. Pure hydrogen gas is used to allow only self-trapping, whereas a mixture of hydrogen and 1% nitrogen is used to enable ionization-induced trapping.

The electrons accelerated in the interaction co-propagate with the laser pulse along the optical axis onto a scintillating screen (Kodak Lanex regular), covered with an aluminum foil that blocks the laser light. The light emitted from the rear side of the scintillating screen is recorded using a 16-bit CCD-camera, and the total response of the system is calibrated and used together with published calibration factors for the screen [18] to determine the amount of charge in the beams of electrons impacting on the screen. Furthermore, a dipole magnet is mounted on a manual linear translation stage and can be moved into the electron beam under vacuum to disperse the electrons depending on their energy. Numerically tracing the electrons through the dipole magnetic field allows electron energy spectra to be determined from the acquired images of the dispersed electrons impacting the scintillating screen.

Before acquiring a series of data, the longitudinal laser focus position, with respect to the gas cell is fine tuned, either by moving the cell or by changing the curvature of the deformable mirror, to yield the best quality of the beams of accelerated electrons. Similarly, the pulse compression is optimized by fine tuning the grating separation.

## 3. Experiments and results

### *3.1. Self trapping and ionization-induced trapping*

The inner length of the cell, i.e. the distance between the inner surfaces of the front and back windows, is set to 2 mm and a sequence of shots is recorded while the backing pressure supplied to the gas cell is varied using either pure hydrogen or a gas mixture containing 1% of nitrogen.

As shown in figure 2(a), the electron number density threshold for trapping of electrons is significantly lower for the gas mixture than for pure hydrogen. This is expected, since the threshold for ionization-induced trapping is lower than for self-trapping [19]. Furthermore, it is observed that the threshold for trapping is much sharper in the case of self-trapping in pure hydrogen than for ionization-induced trapping in the gas mixture. Using the gas mixture at low electron number density, $4 \times 10^{18}$ cm$^{-3}$ to $7 \times 10^{18}$ cm$^{-3}$, the amount of charge in the beams of accelerated electrons scales almost linearly with the electron number density in the plasma, indicated by the red dashed line in figure 2(a). The shot-to-shot fluctuations in charge, as deviations from a fitted linear dependence on the density, is only 1.2 pC here. At higher electron number densities the charge increases more rapidly with density but the relative shot-to-shot fluctuations in charge remains low, and is on average 14.5% at each selected value of electron number density.

A typical image of a dispersed electron beam accelerated when the cell is filled with the gas mixture to provide

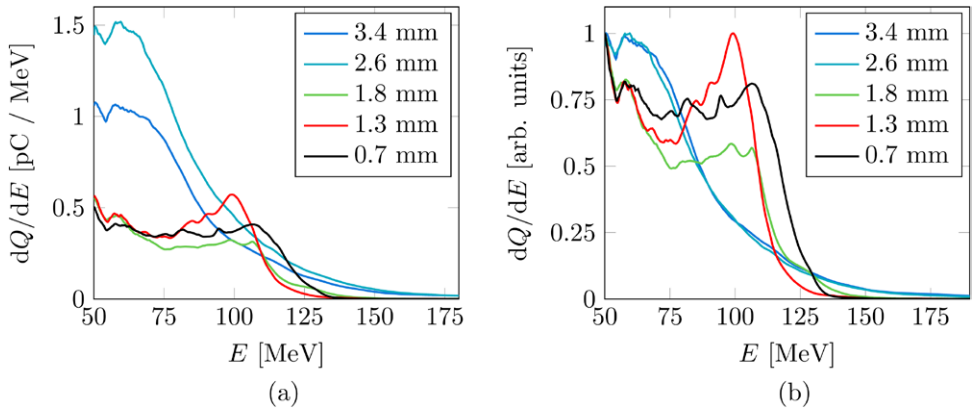


**Figure 3.** (a) Evolution of the electron energy spectrum for beams accelerated using the gas mixture at an electron number density of $12 \times 10^{18}$ cm$^{-3}$ as the length of the gas cell is varied. A peaked feature is observed for cell lengths between 0.7 mm and 1.8 mm. The visibility of the peaked feature is highest at a cell length of 1.3 mm as shown in (b) where the spectra are normalized at 50 MeV. For longer cells the amount of charge is larger but no peak is observed in the electron energy spectra.

an electron number density of $9 \times 10^{18}$ cm$^{-3}$ is shown in figure 2(b). This image shows the reproducible features of the beams of accelerated electrons trapped by ionization, with a large energy spread up to a cut-off energy of approximately 150 MeV and a rather large divergence that is increasing with electron energy (≈12 mrad at 100 MeV). The beam charge, of electrons with energy above 50 MeV, is in this case 38 pC.

Beams with similar amount of charge are produced using pure hydrogen at a higher electron number density, $13 \times 10^{18}$ cm$^{-3}$. A typical image of a dispersed electron beam accelerated under these conditions is shown in figure 2(b). Due to oscillations of the peak normalized vector potential, $a_0$, these beams typically contain multiple, peaked, components as self trapping occurs at multiple locations along the plasma and the energy and number of peaks are fluctuating from shot to shot. Each of these components has an energy spread of about 10% and a divergence smaller than 10 mrad.

### *3.2. Trapping in a density down-ramp*

The length of the cell is varied in a sequence of shots with the cell filled with the gas mixture of hydrogen and 1% of nitrogen and the typical spectral shapes are studied. The electron number density is set to $12 \times 10^{18}$ cm$^{-3}$ to operate the accelerator well above the threshold for ionization-induced trapping [20]. At this density, the power of the laser pulse exceeds the critical power for self-focusing, $P/P_c \approx 4$. The peak normalized vector potential is therefore expected to increase rapidly as the laser pulse enters the gas cell and reaches approximately the value for a matched pulse, for which the transverse size of the laser pulse is approximately equal to the transverse size of the electron void. For a laser pulse containing 585 mJ of energy this corresponds to $a_0 = 3.2$, according to the theory by Lu *et al* [21]. Under these conditions, the dephasing length is $L_d \approx 0.6$ mm. Thus, for regular ionization-induced trapping, broad electron energy spectra, without peaked features are expected.

In figure 3(a), spectra are shown for five shots at different inner cell lengths. For inner cell lengths of above 1.8 mm, the electron energy spectra are wide and monotonically decreasing with energy. For cell lengths of 1.8 mm and lower, the charge distribution is modified and a peak builds up at energies around 100 MeV. The visibility of the peak is largest for a cell length of 1.3 mm as made clear in figure 3(b), in which the spectra are normalized to the charge at 50 MeV.

For cell length below 1.8 mm, it is observed that the shape of the distribution is not sensitive to the cell length and with a peak in the range 100–110 MeV, which suggests that the distance from the point of trapping to the end of acceleration is unaffected by changes in the cell length. This is consistent with the assumption that these electrons are trapped in the density down-ramp at the back of the gas cell.

For a cell length of 0.7 mm, after re-optimizing both longitudinal laser focus position, using the deformable mirror, and pulse compression by adjusting the grating separation, and after decreasing the electron number density to $9.6 \times 10^{18}$ cm$^{-3}$, the peaked features in the spectrum are even more clear (see figure 4(a)). In addition, another peaked feature at higher energy is observed. The peak at lower energy is reproducible and appeared in 73 of 100 shots in a sequence. For these shots the energy of the peak is 90 MeV ± 10% and the energy spread is 20 MeV ± 48%. For the remaining 27 shots, a component at similar energy and divergence is still observed, but is not contributing to a peak in the spectrum but rather a wide distribution of energies up to ≈ 120 MeV. In both cases the divergence was only approximately 3 mrad.

The peak at higher energy is observed on all shots in this sequence at an energy of 150 MeV ± 7%, with an energy spread of 50 MeV ± 18%. This second peaked feature has a larger divergence (≈10 mrad) than the component at lower energy. The total amount of detected charge is on average 9 pC ± 28% in this series of shots.

Under the same conditions, but switching to pure hydrogen, only the peak at 150 MeV remain, as shown in figure 4(b). In this series of shots, the amount of charge is on average 1.0 pC ± 29%, but increases to 2.0 pC when moving the cell only 0.25 mm along the optical axis.

Typical spectra from the two cases, normalized at the peak at high energy, are shown in figure 4(c). Here it can be observed that the energy spread of the component at 150 MeV

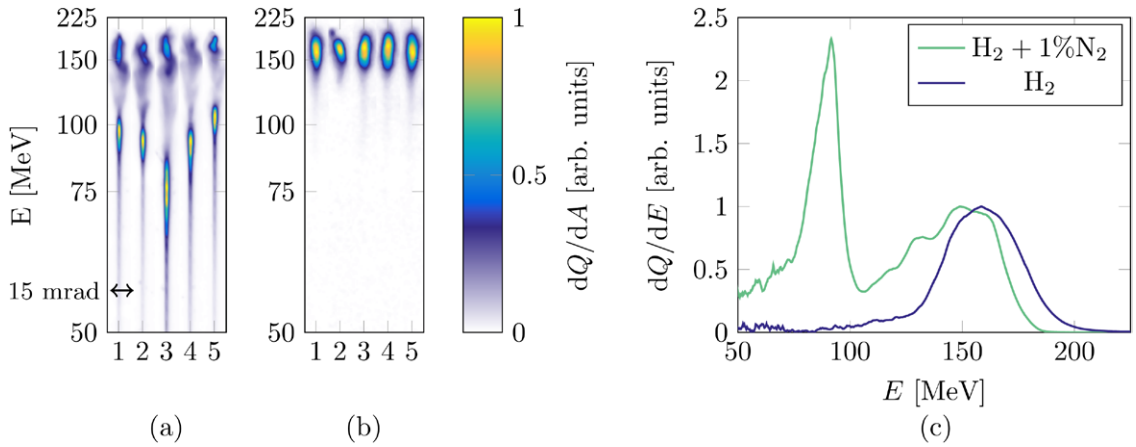


**Figure 4.** Typical traces of the dispersed electron beams using (a) a mixture of hydrogen and 1% nitrogen and (b) pure hydrogen, at an electron number density of $9.6 \times 10^{18}$ cm$^{-3}$ in a cell with an inner length of 0.7 mm. Each trace is normalized to its peak value. The total amount of detected charge is 9 pC $\pm$ 28% in the case of the gas mixture and 1.0 pC $\pm$ 29% in the case of the pure hydrogen. Typical energy spectra of beams of electrons accelerated in pure hydrogen and in a mixture of 1% nitrogen in hydrogen are shown in (c). The energy spectra of all beams feature a peak at approximately 150 MeV. In addition, the beams accelerated in the gas mixture typically contain another peak at a lower energy ($\approx$ 90 MeV). Each curve is normalized to its corresponding value at the peak around 150 MeV, to allow the shapes to be compared.

is approximately 50 MeV (FWHM) in both cases. The component at low energy, for this shot at 90 MeV, has a significantly smaller energy spread of only 15 MeV.

### *3.3. Three-dimensional particle-in-cell simulations*

Simulations are performed using the fully relativistic three-dimensional particle-in-cell code CALDER-CIRC [22], which is exploiting the fact that only a low number of azimuthal Fourier components are required to model laser wakefield acceleration. In the simulations the time step is set to 52 attoseconds and a window following the laser pulse, with a size of 50 $\mu$m longitudinally and 75 $\mu$m radially, is used. The spatial grid size is set to 16 nm in the longitudinal direction and 190 nm in the radial direction, and three azimuthal Fourier modes are used.

The laser pulse is defined in the simulations to have a pulse duration of 34 fs and a transversal size of 17 $\mu$m (FWHM) when focused in vacuum, with a peak normalized vector potential of 1.25, approximately corresponding to laser parameters in the experiment. The waist of the laser beam, when not affected by the propagation in the plasma, is chosen in the simulations to be located at the beginning of the density plateau inside the cell. Furthermore, the shape of gradients of the density distribution in the entrance and exit of the cell are fitted as piece-wise linear functions, consisting of three parts, from the results from the characterization of the gradients using computational fluid dynamics. The length of the gradient is chosen to be 500 $\mu$m, in the fall from 90% to 10% of the plateau density, which corresponds to the shortest possible gradient determined using computational fluid dynamics.

First, simulations are performed at different electron number densities to determine the threshold of self trapping in the density plateau. A simulation is then performed for a cell with an inner length of 0.8 mm at an electron number density of $9.1 \times 10^{18}$ cm$^{-3}$ to avoid self-trapping in the density plateau. The results from this simulation are summarized in figure 5 (a). Here, the evolution of the electron energy spectra are shown for the electrons released by ionization from H and $N - N^{4+}$ in black (upper) and the electrons released by ionization from $N^{5+}$ and $N^{6+}$ green (lower). Also, the evolution of the peak normalized vector potential inside the plasma is shown in red and the electron number density is shown in blue. Each of these curves are normalized to the corresponding maximum value of the simulation. Furthermore, in figures 5(c) and (d), the electron distribution is shown, both in real space and longitudinal phase-space, close to the laser pulse before (b), in the middle (c) and in the end (d) of the density down-ramp together with the corresponding electron energy spectrum at each position.

Under these conditions, ionization-induced trapping occurs continuously in the plateau between the input and exit of the cell and provide a wide, but very weak, background in the electron energy spectrum.

An increased rate of trapping of electrons is observed in the density down-ramp, both for electrons from the background plasma and for electrons ionized from $N^{5+}$ and $N^{6+}$. The electron energy spectrum at the end of the density down-ramp contains two slightly separated peaks, consistent with the experimental results. The peak at higher energy is identified to contain electrons from ionization of hydrogen and from the first ionization states of nitrogen ($N - N^{4+}$). These electrons are released into the plasma, by ionization from their corresponding atoms or ions, far from the peak of the laser pulse, and the simulation shows that these electrons are injected and trapped in the density down-ramp at the exit of the gas cell by density down-ramp injection. The spectral peak at lower energy is due entirely to electrons from ionization of $N^{5+}$ and $N^{6+}$, which occur much closer to the peak of the laser pulse. The simulation shows that these electrons are also trapped in the density down-ramp at the exit from the gas cell.

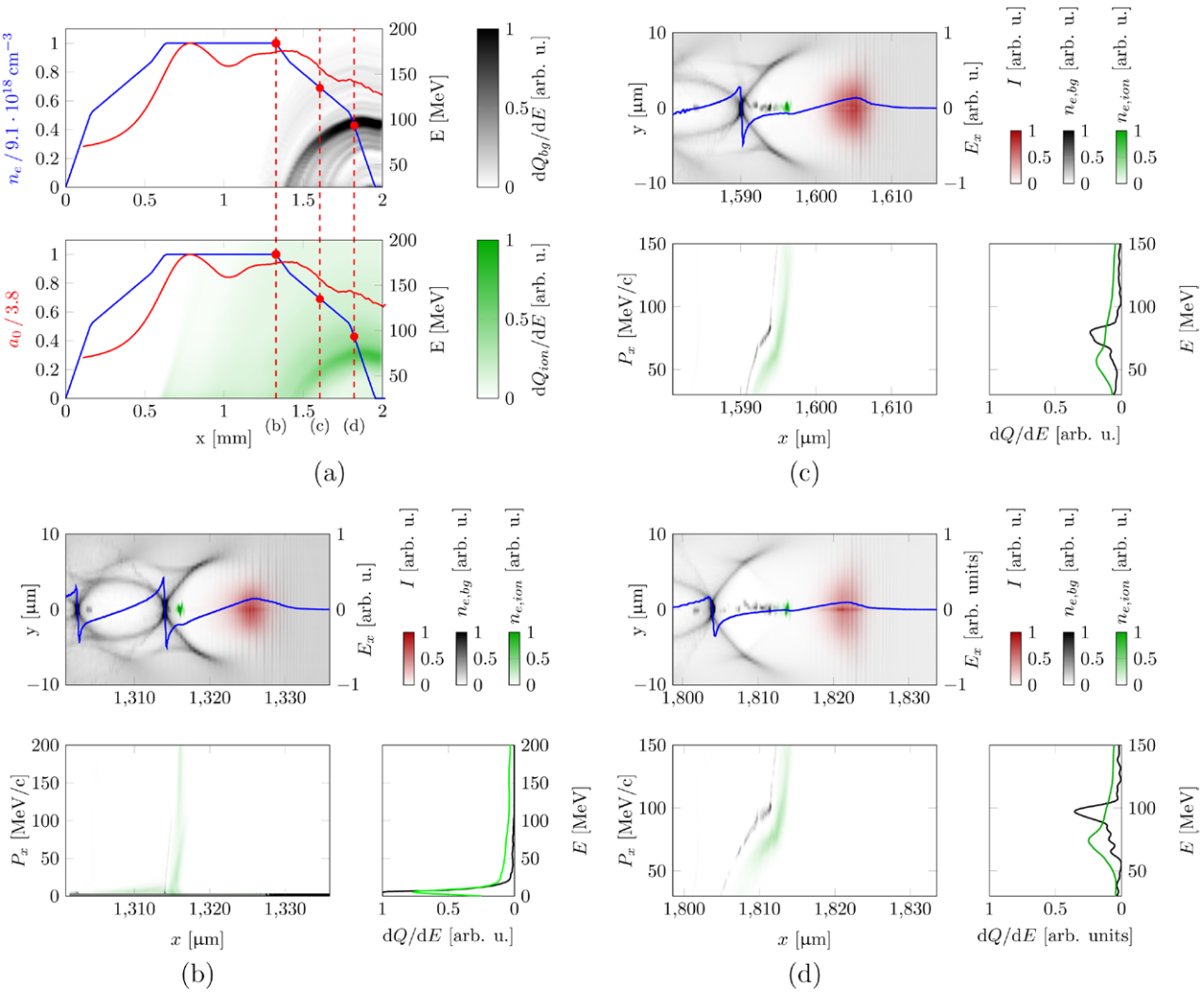


**Figure 5.** Summary of a particle-in-cell simulation (a) showing the evolution of the spectrum of the trapped electrons released by ionization from H and $N - N^{4+}$ (black) and from $N^{5+}$ and $N^{6+}$ (green). Three snapshots ((b)–(d)) from the simulation showing trapping of electrons in the density down-ramp at the exit of the cell, with the corresponding position of each snapshot marked in the density profile in (a). For each snapshot, the density distribution of the background electrons is shown in black, and the electrons released from $N^{5+}$ and $N^{6+}$ in green. The intensity distribution of the laser pulse is shown in red. Before the density down-ramp (b), only a small fraction of electrons, mainly released by ionization of $N^{5+}$ and $N^{6+}$, has been trapped. The electrons released from H and $N - N^{4+}$ and trapped in the density down-ramp (c) are well separated in phase-space from the electrons released from $N^{5+}$ and $N^{6+}$ that are also trapped in this ramp. After further acceleration, and phase-space rotation due to the longitudinal extent of the injected electrons, these two populations form two peaks in the energy spectrum (d).

The simulation further reveals a longitudinal separation of the electrons that build up the two components after they have been trapped in the plasma wave. During the subsequent acceleration in the density down-ramp, the electrons from ionization of $N^{5+}$ and $N^{6+}$ are located closer to the center of the electron void, and thus experience a lower accelerating field than the trapped electrons ionized from H and $N - N^{4+}$, which are located further to the back of the electron void.

The reason for this separation is a fundamental difference in the injection and trapping mechanism. The electrons, already released from the atoms far from the peak of the laser pulse, are injected at the back of the electron void following the laser pulse, as the size of the bubble is growing in the density down-ramp. In contrast, ionization of $N^{5+}$ and $N^{6+}$ releases electrons into the plasma closer to the peak of the laser pulse and they are able to pass through the rest of the laser field into the electron void. The released electrons are then accelerated by the longitudinal electric field and catch up with and exceeds the speed of the laser pulse (corresponding to a relativistic factor $\gamma_l \approx 14$).

Overall, the final electron energy spectrum of the simulation agrees qualitatively well with the experimental findings under similar conditions. However, the energy of the two spectrally peaked features are lower than observed in the experiments. We attribute those differences to discrepancies in the parameters of the laser pulse and/or density distribution between the experiment and simulation. In particular, the effect of a longer density ramp is two-fold: (I) the effective length of acceleration becomes longer. (II) The plasma wavelength is increasing more slowly, which means that the dephasing of the electrons due to the expansion of the plasma wave is slower.

## 4. Discussions

Our experiment using a gas mixture shows two different regimes of laser wakefield acceleration of ionization-induced trapped electrons. For cells longer than approximately 2 mm, a large number of electrons are trapped by ionization-induced trapping, after self-focusing of the laser pulse, in the density plateau. This process occurs over an extended length, as long as the conditions for trapping are fulfilled, and the resulting electron energy spectra are therefore wide without peaked features. Under these conditions, the threshold, in electron number density, for ionization-induced trapping is lower than for self-trapping. For electron number densities in the range between $4 \times 10^{18}$ cm$^{-3}$ and $7 \times 10^{18}$ cm$^{-3}$, the amount of charge in the bunches of accelerated electrons scales linearly with electron number density in the plateau, with only small shot-to-shot fluctuations. This regime is therefore favorable when good control over the charge is desired, but has the drawback of generating beams of electrons with wide energy spectra.

For shorter cells, only few electrons are trapped in the density plateau and provide broad and weak distributions in the energy spectra. However, the density down-ramp at the exit of the cell increases the rate of trapping by ionization, as observed in the simulations. The reason for this increased rate of trapping is the decreased phase velocity of the wake, as the wake period increases behind the laser pulse as it propagates through the density down-ramp, which facilitates trapping of electrons. The region from which electrons can be ionized to become trapped in the wake therefore locally increases in a density down-ramp. Localization of the trapping, together with phase-space rotation of the distribution of trapped electrons [7], yield a peak in the electron energy spectrum.

Similarly, the threshold for trapping of electrons from the background plasma also decreases in the density down-ramp at the exit of the cell, and these trapped electrons also contribute to a peak in the electron energy spectrum (see figures 4(b) and (c)). The electrons trapped from the background plasma are subject to a stronger accelerating field in the wake which results in a higher energy for these electrons compared to the electrons from ionization from $N^{5+}$ and $N^{6+}$.

While the electron energy is higher for the electrons trapped from the background plasma in the density down-ramp, the amount of charge is significantly higher when also ionization-induced trapping occurs in the density down-ramp.

Due to pump depletion, as the length of the cell is increased, the strength of the laser pulse as it reaches the exit down-ramp is decreased. Therefore, the amount of charge injected in the down-ramp is expected to decrease, which agrees well with our observation of no peaked features for cells longer than approximately 1.8 mm.

## 5. Conclusions

We have shown experimentally, and supported by simulations, that the advantage of ionization-induced trapping to provide high charge in beams of accelerated electrons can be combined with a density down-ramp to localize the injection and thereby providing peaked electron energy spectra. Higher charge in the accelerated beams, as compared to pure density down-ramp injection, also implies a better efficiency of the accelerator. The peak energy of the electrons trapped by field ionization of $N^{5+}$ and $N^{6+}$ at the back of a gas cell shows only small shot-to-shot fluctuations and the method is therefore a suitable choice for a stable wakefield accelerator.

## Acknowledgments

We acknowledge the support of the Swedish Research Council, the Knut and Alice Wallenberg Foundation, the Swedish Foundation for Strategic Research, the Triangle de la Physique (Grant Agreement No. 2012-032TELISA), Laserlab-Europe/LEPP (Grant Agreement No. 654148, EC's Horizon 2020) and EuCARD2/ANAC2 (Grant Agreement No. 312453, EC's 7th Framework Programme). The simulations were performed on resources provided by the Swedish National Infrastructure for Computing (SNIC) at Lunarc. SR acknowledges support from the ERASMUS programme.

## References

[1] Faure J, Glinec Y, Pukhov A, Kiselev S, Gordienko S, Lefebvre E, Rousseau J P, Burgy F and Malka V 2004 *Nature* **431** 541–4
[2] Geddes C G R, Toth C, van Tilborg J, Esarey E, Schroeder C B, Bruhwiler D, Nieter C, Cary J and Leemans W P 2004 *Nature* **431** 538–41
[3] Mangles S P D *et al* 2004 *Nature* **431** 535–8
[4] Tajima T and Dawson J M 1979 *Phys. Rev. Lett.* **43** 267–70
[5] He Z H, Thomas A G R, Beaurepaire B, Nees J A, Hou B, Malka V, Krushelnick K and Faure J 2013 *Appl. Phys. Lett.* **102** 064104
[6] Leemans W P *et al* 2014 *Phys. Rev. Lett.* **113** 245002
[7] Hansson M, Aurand B, Davoine X, Ekerfelt H, Svensson K, Persson A, Wahlström C G and Lundh O 2015 *Phys. Rev. ST Accel. Beams* **18** 071303
[8] Hansson M *et al* 2014 *Phys. Rev. ST Accel. Beams* **17** 031303
[9] Faure J, Rechatin C, Norlin A, Lifschitz A, Glinec Y and Malka V 2006 *Nature* **444** 737–9
[10] Schmid K, Buck A, Sears C M S, Mikhailova J M, Tautz R, Herrmann D, Geissler M, Krausz F and Veisz L 2010 *Phys. Rev. ST Accel. Beams* **13** 091301
[11] Burza M, Gonoskov A, Svensson K, Wojda F, Persson A, Hansson M, Genoud G, Marklund M, Wahlström C G and Lundh O 2013 *Phys. Rev. ST Accel. Beams* **16** 011301
[12] Gonsalves A J *et al* 2011 *Nat. Phys.* **7** 862–6
[13] Golovin G, Chen S, Powers N, Liu C, Banerjee S, Zhang J, Zeng M, Sheng Z and Umstadter D 2015 *Phys. Rev. ST Accel. Beams* **18** 011301
[14] McGuffey C *et al* 2010 *Phys. Rev. Lett.* **104** 025004
[15] Desforges F G *et al* 2014 *Phys. Plasmas* **21**
[16] Mirzaie M *et al* 2015 *Sci. Rep.* **5** 14659
[17] Thaury C *et al* 2015 *Sci. Rep.* **5** 16310
[18] Buck A *et al* 2010 *Rev. Sci. Instrum.* **81** 033301
[19] Pak A, Marsh K A, Martins S F, Lu W, Mori W B and Joshi C 2010 *Phys. Rev. Lett.* **104** 025003
[20] Chen M, Esarey E, Schroeder C B, Geddes C G R and Leemans W P 2012 *Phys. Plasmas* **19** 033101
[21] Lu W, Tzoufras M, Joshi C, Tsung F S, Mori W B, Vieira J, Fonseca R A and Silva L O 2007 *Phys. Rev. ST Accel. Beams* **10** 061301
[22] Lifschitz A, Davoine X, Lefebvre E, Faure J, Rechatin C and Malka V 2009 *J. Comput. Phys.* **228** 1803–14